DESIGN OF A HYBRID ELECTRIC UAV THROUGH MULTI-OBJECTIVE OPTIMISATION

Teresa Donateo [a], Claudia Lucia De Pascalis [b], Antonio Ficarella
Dept. of Engineering for Innovation, University of Salento, Lecce, Italy
ITALY

[a] teresa.donateo@unisalento.it, [b] claudia.depascalis@unisalento.it

Keywords: Hybrid electric aircraft. UAV. Energy management strategy. Wankel engine. Scaling models.

ABSTRACT

Problem and purpose *- In order to exploit the potentiality of hybridization and quantify the environmental advantages obtainable with today technologies while waiting for innovations in batteries and electric machines, it is necessary to develop advanced numerical tools that takes into account the size of the components, the energy management strategy, the flight trajectory, etc. This problem is addressed here through the application of multi-objective optimization methods to a parallel hybrid electric power system based on a Wankel engine.* ***Methodology*** *- The power request at propeller axis of each flight segment is used to calculate the overall fuel consumption of the mission (Mfuel) and the maximum payload weight (Wpay) through an average-point analysis. These outputs depend on the size of the components and on the energy strategy that is expressed by the power-split ratio of each mission phase between engine and motor.* ***Originality*** *– The novelty of the investigation is twofold: the application of hybridization to a Wankel engine for which a scaling method is proposed, and the inclusion of the energy management in the design of the power system.* ***Main findings*** *– Compared with a conventional power system based on a 56kW Wankel engine, a 3.24% saving of the fuel mass burned throughout the mission was found (allowing a -3.25% in total emissions of CO_2 and a 2.34% reduction of the cost-per-mission).* ***Limitations and recommendations*** *- The method is based on simplified models, in particular for the electric machine and the propeller. Moreover, the scaling method uses a limited database of Wankel engines that, unlike piston engines, are a technology not yet fully consolidated.*

1.0 INTRODUCTION

In the last decade, concepts of power systems electrification have earned an increasing interest due to their several benefits, such as higher power-to-weight ratio, reliability, compactness, and quietness with respect to the conventional configurations, and, above all, pollutant emissions cutback. Furthermore, other advantages may be the reduction of thermal and acoustic signature thanks to the possibility to fly in electric mode and the possibility to exploit electrification to improve the performance of the vehicle in terms of take-off distance or the service ceiling (Donateo et al. 2018). Among these reasons, a particular relevance is worn by the reduction of noise and emissions.

Electric architectures for aircraft propulsion can be divided in four main configurations: full-electric, turbo-electric, series and parallel hybrid-electric. Pornet et al., 2015 classified them in terms of energy and power hybridization factors, whose latter is defined in Eqn (1).

$$HF = \frac{P_{EM}}{P_{TOT}} = \frac{P_{EM}}{P_{ICE} + P_{EM}} \tag{1}$$

where P_{EM} is the power delivered by the motor, P_{ICE} is the power from the engine, and P_{TOT} is the total quantity of mechanical power generated at propeller by the hybrid architecture. (Pornet et al., 2015).

Previous investigations of the authors demonstrated that large improvements can be obtained by exploiting synergies between powertrain, aircraft structure, and mission during the design process of electric and hybrid-electric aircraft (Donateo et al., 2018; Donateo et al.,2019). This is even truer if new powerful concepts are involved in the design process too, such as optimization, control, integration, multi-functionalization, distributed propulsion, etc. As a step further, this investigation focuses on the key role of energy management in hybrid electric systems that is called to define, at each step of the mission, how to use the energy stored in the battery.

To exploit the synergy between configuration and energy management, it is possible to consider four approaches (Silvas et al. 2016). In this study, it is considered a "Simultaneous design-control optimization approach", which performs a simultaneous optimization of plant and controller. It differs from the method previously proposed (Donateo et al.,2018) because the mission is not discretized into small time steps like in the automotive case but subdivided in phases and segments (more suitable to the aircraft field).

This study defines a method of sizing parallel hybrid-electric power systems for UAVs (aircraft, in general) involving the optimization of the energy management strategy throughout the mission by means of the use of the powerful tool of the multi-objective evolutionary algorithms. The method is here applied to a tactical UAV with an installed power below 70kW, an application where Wankel engines are preferred. Therefore, another novelty of this investigation is the development of a model for this kind of engine that is able to estimate the fuel consumption in each mission segment according not only to the flight conditions of the segment but also to the size of the engine.

2.0 UAV HYBRIDIZATION

In the paper of Oron, 2016, a classification of the UAVs propulsion system is presented relying on the power request (BHP). In particular, electric propulsion is preferred when BHP does not exceed few kilowatts, positive displacement engines are used between 12 and 190kW, and gas turbine engines for higher power ranges. The hybridization of a Medium-Altitude Medium-Endurance (MAME) UAV with a power range where Wankel engines are preferred (15 to 70 kW) is considered here. Note that Wankel engines are advantageous in terms of high-speed, regularity of operation, limited number of components, modularity and power-to-weight ratio but are penalized by poor fuel economy with respect to reciprocating engines (Lu Y et al. 2019). Therefore, hybridization can be particularly effective in Wankel-based UAVs.

For the powertrain hybridization, a parallel configuration is preferred against a series one, because of the higher overall efficiency and the lower number of components. A parallel hybrid-electric powertrain configuration (Figure 2-1) consists of a Wankel engine and a permanent magnet electric machine mechanically connected to the propeller. Lithium-polymer batteries are considered here as representative of today technology for electric storing.

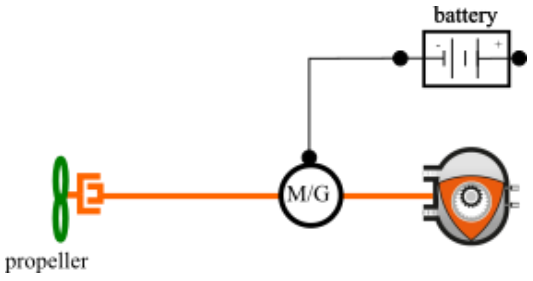

Figure 2-1 Parallel hybrid-electric powertrain configuration

If U is the power-split ratio that define the amount of the mechanical power to be delivered by the electric branch of the hybrid system, the following energy mode are possible:
1. Thermal: the engine produces all the mechanical power required (U=0);
2. Electric: the propeller shaft power is generated by the motor using the battery as only energy source (U=1);
3. Charging: the engine generates the power to move the propeller and to charge the battery, while the electric machine works as a generator (U<0);
4. Power-assis: both the engine and the motor generate mechanical power that is delivered to the propeller (0<U<1).

It is important to clarify the meaning of the following terms that will be used later in this paper:
- "phase" defines the mission in terms of take-off, climb, cruise or loiter, descent, landing;
- "segment" refers to the discretization of the mission for the energy analysis (take-off, Nsegm segments of 720 seconds, landing);
- "piece" refers to a part of mission grouping adjacent segments characterized, without interruption, by the same energy mode.

3.0 THE MODELLING APPROACH

The energy analysis of the systems is based on the propulsive power that is calculated by applying the balance of the forces acting on the plane in each phase of the mission (according to the mission profile). Then, each component of the power system is simulated as a black box. The propeller, the thermal engine and the electric machine are treated as energy converters. The input of each energy converter block is the power required by the component (according to the mission and/or the energy management strategy) while the output is the power needed for the conversion. The efficiency of the propeller is arbitrary set at each phase according to the authors' experience. The electric motor (as both motor and generator) and the thermal engines are modelled with the Willans line approach (Guzzella and Sciarretta 2007) that calculates the output power of an energy converter as in Eqn (2).

$$P_{out} = e \cdot P_{in} - P_0 \tag{2}$$

where P_{in} is the chemical power in case of engines (P_{chem}) and the electric power in case of motors, "e" is the intrinsic "indicated" efficiency of the energy converter, while P_0 includes the losses occurring after the energy conversion. For permanent magnet electric machines in the range of 30kW, Guzzella et al. 2007 proposes e=0.96 and P_0=1.4kW. For thermal engines, the two parameters of the model are usually expressed as a function of engine speed and load and strongly depend on engine technology
The battery is treated as a reversible energy storage system and simulated with an electric circuit equivalent model when in discharge while recharging is simulated with an empirical model. Both models were extensively validated with experimental data on Lithium-polymer batteries (Donateo et al. 2018).
More details are needed for the scalable model for the Wankel engine. The concept of scalability is meant as the possibility to obtain a good estimation of the behaviour of an energy device starting form data of a reference device with the same technology but different size. This aspect is crucial in the sizing of a hybrid electric power system. In this investigation, we use as reference engine the AR682 of UAV Engines LTD because of the availability of information on this engine. The datasheets of other Wankel engines of the same manufacturer (https://uavengines ltd.co.uk/products/ar682-75-bhp/) are used for the validation Table 3-1.

The procedure is based on the assumption that all engines belonging to the same technology (spark ignited rotary engines in this case) have similar values of brake mean effective pressure bmep and tangential rotor speed vr and the same efficiency map in terms of bmep and vr . Therefore, the engine brake power is proportional to its displacement while the revolutions per minutes are inversely proportional to the engine size.

Table 3-1: UAV's Wankel engines specifications from manufacturer

Engine	Number of rotors	Displacement	Power output	Mass	Nominal SFC
AR682	2	294 cc	56 kW @ 6000 rpm	51.0 kg	316.3 g/kWh
AR682R	2	294 cc	67 kW) @ 7000 rpm	56.5 kg	334.6 g/kWh
AR741	1	208 cc	28 kW @ 7800 rpm	10.7 kg	346.7 g/kWh
AR801R	1	294 cc	38 kW @ 8000 rpm	25.4 kg	316.3 g/kWh

The procedure starts form a tentative value of the displacement (disp) and iterates on it until the resulting nominal power ($P_{ice,n}$) meets the desired value, through the computation of the engine rev per minute (n_{ice}). Knowing disp and n_{ice} lets get the engine number of rotors (N_{rot}), which is considered to be proportional to disp and a multiple of half number of the reference engine rotors. Finally, the second and last iteration is performed on disp (and, consequently, on n_{ice}) with the new value of N_{rot}, returning the definitive values of disp, n_{ice} and N_{rot}. For the Wankel engine, a constant power-to-weight ratio of 1 kW/kg is assumed. The engine volume is assumed proportional to the product of displacement and number of rotors. Figure 3-1 shows that the scaling procedure allows the estimation of the engine specification as a function of the desired nominal power with a reasonable accuracy.

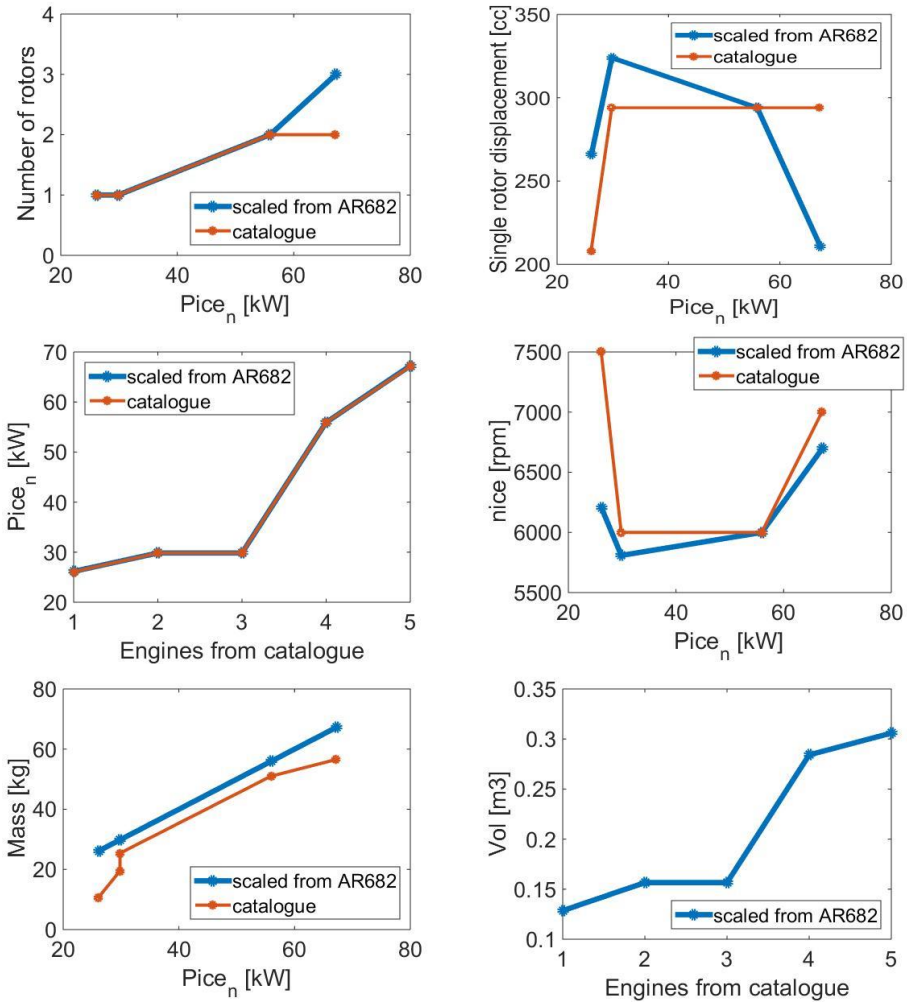

Figure 3-1: Model validation (Scalability)

Once the size of the engine has been defined, its specific fuel consumption at each segment is calculated as a function of altitude and power request while the engine speed is set equal to its nominal value ($n_{ice}(isegm)=n_{ice}$). To account for the scalability, the Willans line model is expressed in terms of brake mean effective power (bmep) and available mean effective power (amep) defined as in Eqns (3) (4).

$$bmep = \frac{P_{ice}(isegm)}{disp \cdot n_{ice}(isegm)/60} \tag{3}$$

$$bmep = \frac{P_{chem}(isegm)}{e_{wl}} = \frac{w_{fuel}(isegm) \cdot LHV}{e_{wl}} \tag{4}$$

where w_{fuel} (isegm) is the fuel flow rate of the segment isegm and LHV is the lower heating value of the fuel.

The numerical coefficients of the model (Eqn (5)) are obtained by fitting the SFC map that was made available by the manufacturer for the AR682 engine as explained in Figure 3-2:

$$bmep = e(n_{ice}) \cdot amep - p_0(n_{ice}) \tag{5}$$

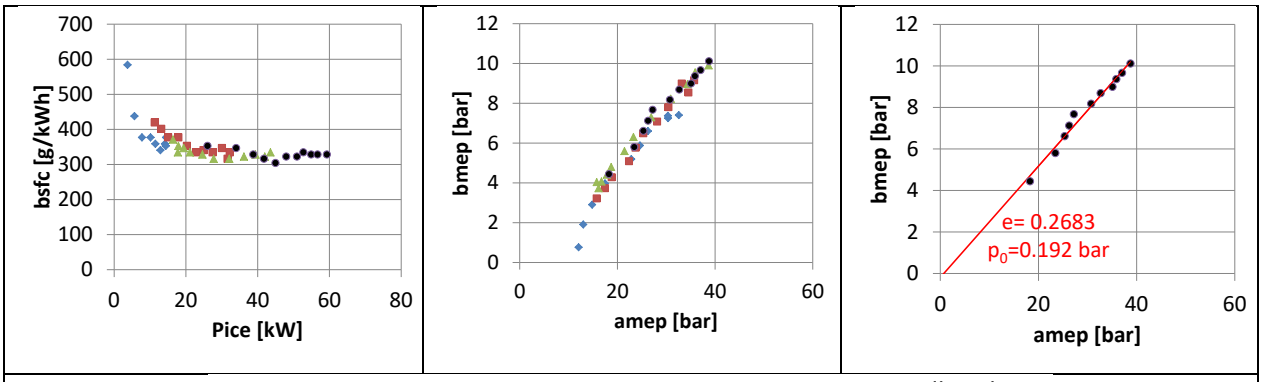

a) data of SFC versus speed and power as given by AR682 manufacturer	b) representation of the available data as scalable quantities at different engine rpm	c) Willans line as linear interpolation of available data (at 6000 rpm)

Figure 3-2: Fitting procedure to derive the coefficients of the Willans line at different engine peed

Finally, the performance of the engine and its efficiency at high altitude are different from sea level (SL). As known in literature, (McCormick, 1995) a "corrected density" (σ) can be used to decrease bmep according to the atmospheric pressure and temperature at flight level z. It is calculated as in Eqn (6).

$$\sigma(z) = \frac{p(z)}{p_{SL}} \sqrt{\frac{T_{SL}}{T(z)}} \tag{6}$$

More details on the correction with altitude and on the validation of this approach can be found in Donateo et al. 2016.

4.0 THE DESIGN APPROACH

The values of the power-split ratio parameter at each mission segment (representing the energy management strategy of the mission) are grouped in the vector U to be optimized, which is defined as in Eqn (7).

$$U(isegm) = \frac{P_{EM}(isegm)}{P_{TOT}(isegm)} = \frac{P_{EM}(isegm)}{P_{ICE}(isegm) + P_{EM}(isegm)} \quad (7)$$

where PEM is the power delivered by the motor, PICE is the power from the engine, and PTOT is the total quantity of mechanical power generated at propeller by the hybrid architecture. Together with U, other design variables are the battery cell capacity (Ccell), the number of battery cells in parallel (np,bat), and the battery rate of charge (crech).

The design method proposed in this study for the parallel hybrid-electric powertrain involves the optimization of the above design variables, aiming at minimize the overall fuel consumption (Mfuel) and maximize the maximum payload weight (Wpay). Constraints about MTOW and the powertrain volume are included because we are replacing a powertrain in an existing aircraft, so having well-defined specifications. Furthermore, a constraint on the engine power is due to the well-known limits of the thermal machines when their size decreases (20 kW $\leq$ $Pice_n$ $\leq$ 90 kW). Other constraints are included in order to check the design feasibility in terms of battery capability to work out the whole mission.

An hypothetical target mission consisting of take-off, first and second climb, outbound segment to reach the operating area, loiter, and landing is considered here based on the information reported in (Donateo et a. 2016). Table 4-1 reports the mechanical power required at each phase. For the design optimization, all the mission phases, except for take-off and landing, are discretised into segments of 720 seconds each having their own value of U(isegm) to be optimized.

Table 4-1: Target mission of the UAV

Flight phase	Mechanical power at propeller [kW]
Take-off	63.4
Climb1	30.8
Climb2	17.2
Outbound	14.1
Loiter	10.8
Descent	11.5
Landing	9.7

Note that the weight of the aircraft during the mission changes according to the time history of fuel consumption. Therefore, the power at propeller axis at each mission segment in the hybrid-electric configuration may vary with respect to the values of Table 4-1, which refer to the baseline power system because of the different fuel consumption. This was taken into account in this investigation by upgrading the power request of each segment according to the fuel consumption in the previous time steps.

Taking as input the mission profile, the optimization design variables, the aircraft MTOW=650 kg and empty weight (Wempty=400 kg, not including the power system contribution), and the power system volume of the baseline configuration (Vref $\cong$ 0.257 m^3, including engine and fuel tanks), an in-house code carries out the sizing of each component of the hybrid-electric power system as follows:

1) At each phase of flight, the mechanical power request is split between the electric and thermal lines as a function of the corresponding value of U(isegm) ;

2) Engine and motor are sized based on the corresponding maximum power request over all segments, letting to estimate their mass and volume;

3) Knowing the engine size and its operating point, it is possible to calculate the amount of fuel consumed during each flight segment;

4) The battery is sized in order to satisfy the electric power and energy required during the whole mission;

5) Mfuel and Wpay are finally computed and constraints are checked out.

Table 4-2 reports all the optimization design variables together with their upper and lower limits.

Table 4-2: Hybrid electric powertrain design variables

Variable	Lower / Upper limits	Notes
U (isegm) for each isegm=1:Nsegm	-0.01 / 1	-0.01=RECHARGE mode 0 THERMAL mode 1 ELECTRIC mode (0,1) POWER-ASSIST mode
Ccell [Ah]	11 / 53	Individual battery cell capacity
np,bat	1 / 15	Number of battery cells in parallel
crech	0.1 / 3	Recharge rate

That procedure is integrated into an optimization environment to exploit the potentiality of Evolutionary Algorithms in finding a Pareto front of optimal solutions with concurrent goals subjected to several design constraints. In particular, a modified version of the S-Metric Selection Evolutionary Multi-Objective Algorithm (SMS-EMOA) (Emmerich et al., 2005) was found to be very helpful in addressing the topic of aircraft electrification (see Donateo et al. 2019).

5.0 COMPONENTS SIZING

When U(isegm) >0 the power to be delivered by motor and engine is calculated according to the value of U(isegm) as in Eqns (8) (9) (10).

$$P_{ice}\ (i\_segm = 1 - U_{segm}\ (i)] \cdot P_{ax,prop}(isegm) \tag{8}$$

$$P_{mot}\ (isegm = U_{segm}(i) \cdot P_{ax,prop}(i\_segm) \tag{9}$$

$$P_{bat}(isegm) = \frac{P_{mot}}{(\eta_{mot})^{\gamma}} \tag{10}$$

where P_{ice}(isegm), P_{mot}(isegm), and P_{bat}(isegm) are the power required from internal combustion engine (ICE), motor, and battery, respectively, at the mission segment isegm while, $P_{ax,prop}$(isegm) is the mechanical power required at the propeller axis. Note that γ is used to identify if the electric machine is working in motor mode (γ=1) or used as a generator (γ=-1). The procedure used when U(isegm) <0 (and γ=-1) is explained later in this section.

The motor volume (Vmot) and mass (Mmot) are calculated as in Eqns (11) (12).

$$M_{mot} = \left(\frac{C_{bat}}{0.0482 \cdot C_{bat} + 1.288}\right) + 0.339 \cdot P_{mot,n} + 5.45 \quad (11)$$

$$V_{mot} = (Vm_0 + C_{bat} \cdot Vm_1) + 0.57 \cdot P_{mot,n} + 7.94 \quad (12)$$

where Vm_0, Vm_1, and the constant values are statistically derived parameters (Donateo et al., 2018) while, $P_{mot,n}$ is the nominal motor power, and C_{bat} is the battery capacity C_{bat}=Ccell·$n_{p,bat}$.

The battery sizing is carried out in two steps. First, it is performed a preliminary estimation of the number of the battery cells in series ($n_{s,bat}$) in order to make the battery able to complete the most expensive segment in term of electricity among those performed in discharge- or power-assist mode. Then, the $n_{s,bat}$ value is refined in order to ensure that the battery SOC never goas below 20%.

The battery capacity at the end of each mission segment (Cf) is computed by using the concept of "effective current" (Ieff), which is the effective battery current taking into account the Peukert's effect (Guzzella et a. 2007), as in Eqn (13)(14).

$$I_{eff}(i) = I_{bat,vect}(i)\left(\frac{I_{bat,vect}(i)}{C_{bat}}\right)^{peuk-1} \quad (13)$$

$$C_f(i) = C_f(i-1) \cdot I_{eff}(i) \cdot t(i) \quad (14)$$

where "peuk" is the Peukert's coefficient (=1.05 for Li-po batteries (Traub 2011)), and "t" is the time vector, including the time length of each mission segment.

After calculating the battery size ($n_{s,bat}$), the actual initial and final capacity of the battery at each mission piece is checked to be greater than 20% of C_{bat}, by taking into account the amount of battery capacity recharged during the mission segments in RECHARGE mode. Otherwise, the solution is treated as unfeasible.

Finally, the battery total voltage (Vbus) is computed as in Eqn (15).

$$V_{bus} = n_{s,bat} \cdot V_{cell} \quad (15)$$

when U(isegm)<0, which means RECHARGE or ON-OFF energy mode, the starting point is the power needed to recharge the battery according to the selected c_rech (see Eqns (16)(17)(19)(20)).

$$P_{rech} = c_{rech} \cdot C_{bat} \cdot V_{bus} \quad (16)$$

$$P_{ice}(isegm) = P_{ax,prop}(isegm) + P_{rech} \quad (17)$$

$$P_{ice,SL} = P_{ice}\frac{p_{SL}}{p_0}\sqrt{\frac{T_0}{T_{SL}}} \quad (18)$$

$$P_{ice,nom} = max\left(P_{ice,SL}\right) \quad (19)$$

$$M_{ice} = P_{ice,nom} \tag{20}$$

where the subscripts “SL” and “0” refer to the sea-level and high altitude conditions, respectively. The nominal power of the engine is computed according to the power that the engine must deliver at sea level.

The engine mass (Mice) and volume (Vice) and its fuel economy in its segment is calculated according to the data of Figure 3-1.

6.0 RESULTS AND DISCUSSION

Figure 6-1a reports the 37 optimal solutions of the Pareto front with bubbles coloured according to the hybridization factor (HF) of each solution, A normalized version of the Pareto front (Figure 6-1b) was used to identify three competitive designs of the power system. In particular, the “Best tradeoff” solution was found by minimizing the distance from an ideal optimal point corresponding to the fuel economy of “Mfuel min” and the payload of “Mpay max”. The preference among the 37 solutions of the Pareto front depends on the weight assigned to each goals by the decision making. In this investigation, we chose “Mfuel min”.

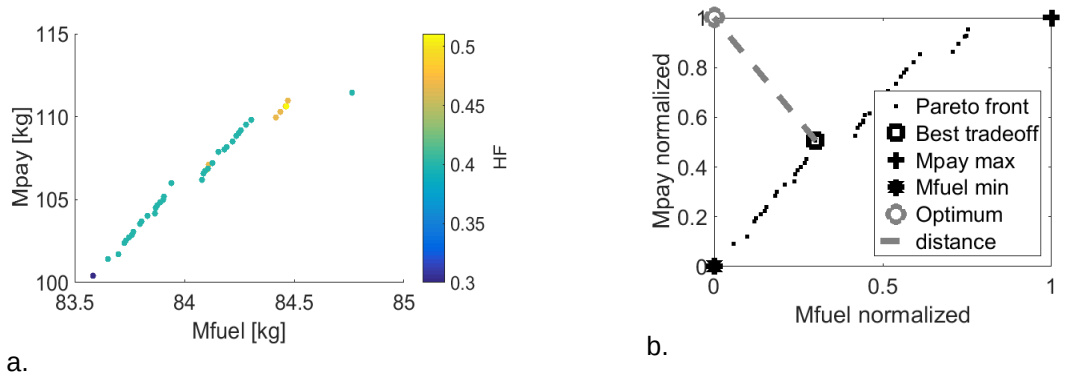

Figure 6-1: Final Pareto front

Table 6-1 reports the values of the design variables in the “Mfuel min” case that will be considered henceforth as “optimal solution”.

Table 6-1: Specification of the optimal solution in terms of design variables

Utakeoff	**Uclimb1(isegm)**			**Uclimb2(isegm)**			**Uoutbound(isegm)**	
0.3	0	0	0	0	0	0	0	0
				Uloiter(isegm)				
0	0	0	0	0	0	0	0	0
0	0	0	0	0	0	0	0	0
0	0	0	0	0	0	0	0.3	0
0	0	0	0	0	0	0	0	0
0	1	0	0					
				Udescent(isegm)			**Ulanding**	
-0.1	-0.1	0	0.2	0	0	0	0.8	
	Ccell			**np,bat**			**crech**	
	11.6 [Ah]			1			0.1	

Table 6-2 reports a comparison between the baseline engine and the optimal hybrid configuration, showing a 3.24% reduction of the overall fuel consumption with respect to the baseline value and about the same maximum-payload mass (+0.2%). The percentage of fuel saving is in line with what found by Frosina et al. in (Frosina et al., 2018).

Table 6-2: Baseline vs Hybrid Electric

Baseline configuration			**Hybrid electric configuration (minimum-fuel point) with today technology**					
Mfuel [kg]	Mpay [kg]	Pice,n [kW]	Mfuel [kg]	Mpay [kg]	HF	ns,bat	Pice,n [kW]	Pmot,n [kW]
86.4	100.2	63.4	83.6 (-3.24%)	100.4 (+0.2%)	0.3	112	44.4	19.0

The optimal battery technology resulting from the optimization is the SLPB065070180, with a energy density of 246.0 Wh/kg / 419 Wh/l, a maximum rate of discharge of 2C and a cell capacity of 11.6Ah.

Note that the power required at each phase of flight by the aircraft with the hybrid configuration is pretty much the same of the baseline case so the correction to the aircraft weight in the different flight segments is quite irrelevant. The engine is strongly downsized with respect to the original configuration (-30% Pice,n) and the optimal hybridization factor for this application, according to the results of this investigation, is therefore HF=0.3.

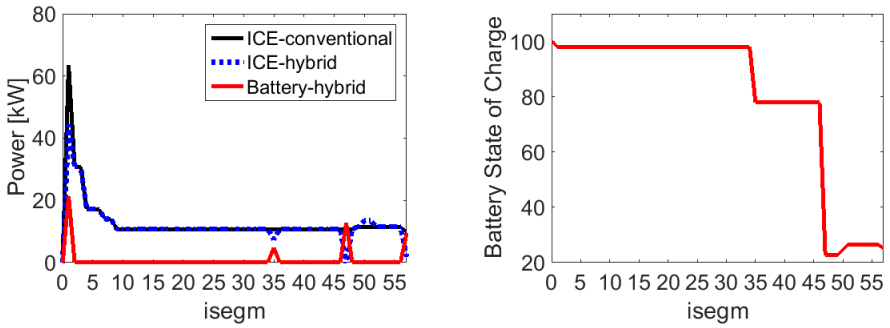

a. **b.**

Figure 6-2: Power split of the hybrid solution versus original (black line) and SOC time history

To better understand how the fuel saving is achieved, Figure 6-2a reports the engine and motor contributions to the mechanical power at each mission segments, while, Figure 6-2b shows the battery state of charge (SOC) at the end of it.
From Figure 6-2, it is evident that the fuel reduction is possible thanks to different effects. The first one is the downsizing of the engine due to the contribution of the battery to the take-off power being the highest value of power request of the mission. This makes the engine work closer to its nominal power during all the other mission segments, which are characterized by much less power request than the take-off phase. In turn, this allows a reduction of the specific fuel consumption (SFC) in those segments and, therefore, of fuel economy. However, the most important contribution to fuel saving is that part of the energy required by the mission is given by the battery that is fully discharged from take-off to landing. Since the two forms of consumption (fuel and electricity) cannot be summed, one can convert them into either CO2 emissions or costs per mission. In this way, it is also possible to better into evidence the environmental and money-saving advantages of hybridization.

6.1 Benefits in terms of environment and costs

The emissions of carbon dioxide of an aircraft can be divided into direct and indirect.

The direct or local emissions are those from the engine during the flight and are directly proportional to fuel flow rate (Eqn (21)).

$$Local\ emissions\ (isegm\ ) = M_{fuel}(isegm\ ) \cdot 8.31 \cdot 0.227 \tag{21}$$

where 0.227 is the conversion factor from gallon to kilogram, and 8.31 kgCO2/gal is the emission factor for AvGas (https://www.epa.gov/sites/production/files/2015-07/documents/emission-factors_2014.pdf).

Indirect or “well-to-tank” emissions are related to the process of obtaining the energy stored in the aircraft in the two forms (fuel and electricity). For the gasoline, they are estimated to be 17% of direct emissions, while 0.3985 kg/kWh is the CO_2 emission factor associated to electricity production in Italy

From this analysis, we obtain 163 kg for the baseline powertrain and 157.7 kg for the hybrid architecture (-3.25% for total emissions).

The costs for fuel and electricity are estimated as in Eqns

$$Baseline\ cost = M_{fuel} \cdot 6.2 \cdot 0.227 \quad (22)$$

$$Hybrid\ cost = M_{fuel} \cdot 6.2 \cdot 0.227 + 0.23 \cdot (C_{bat} \cdot V_{bus})/1000 \quad (23)$$

where 6.2 USD/gallon is an average value of the specific cost of the AvGas in 2015 (https://aviationweek.com/bca/jet-and-avgas-fuel-prices-august-2015), 0.227 is the conversion factor from gallon to kilogram, and 0.23 USD/kWh is the electricity specific cost in Italy (https://www.globalpetrolprices.com/electricity_prices/). Overall, we obtain a reduction by 2.34% also in the cost per mission. In fact, the cost per mission of the baseline case is 121.6 USD while in the case of the hybrid solution we have 118.7 USD.

6.2 Benefits in terms of endurance

The optimization performed here was aimed at improving fuel economy, being the mission the same. However, considering the kind of application, one could choose to use the saved fuel to increase the endurance i.e. the length of the mission. To consider this case, we added to the loiter phase additional segments performed in thermal mode until the total fuel per mission was equal to the baseline case. In this way, we obtained an improvement by about **4.3% in the duration of the loiter (t_{loiter} from 8 to 8.344 h).**

6.3 Benefits in terms of performance

If the battery is sufficiently charged, the hybridization allows a larger free power in each phase that can be used to take-off from a shorter runaway, to climb faster or to increase service ceiling (Donateo et al. 2018).

7.0 CONCLUSIONS

In this study, a design method is proposed for a parallel hybrid electric configuration to replace the conventional thermal engine of a tactical unmanned aerial vehicle (UAV). It consists of the optimization of the energy management strategy used in the different phases of the aircraft flight-path, in order to minimize the overall fuel consumption throughout the mission (Mfuel) and maximize the aircraft maximum payload mass (Mpay). The energy strategy is expressed in terms of the so-called power-split ratio (U(isegm)), which defines how the mechanical power required at propeller is divided between the thermal and electrical branches of the hybrid powertrain at each segment of the mission that is discretised in 55 segments of 720 seconds plus takeoff and landing. The battery is chosen during the design process among a set of existing devices from the Kokam's website. For the thermal branch of the power system, Wankel engines are considered, for which a scaling method is proposed and validated that is used in order to estimate their performances for different sizes starting from a reference device. However, the methodology can be applied to any kind of engine. The optimum found in the optimization is characterized by a power hybridization factor of 0.3 and allow a 3.24 % saving of the fuel mass burned throughout the mission (or, alternative an improvement of endurance by 4.3%) with respect to the same mission run with baseline powertrain with about the same maximum-payload mass (+0.2% of Mpay). This is an important outcome that shows how today technologies can already led to improvements in terms of fuel consumption and emissions, thanks to the possibility to downsize the engine and optimize its usage during the mission. Finally, the fuel economy was also expressed in terms of environmental and economic advantages, giving a 3.25% reduction in emissions of CO2 (direct and indirect) and a 2.34% cutback of the cost-per-mission.

REFERENCES

Brelje, B.J., Martins, J. R.R.A., (2019) “Electric, Hybrid, and turboelectric fixed-win aircraft: A review of concepts, models and design approaches”, Progress in Aerospace Sciences, vol. 104, pp 1-19.

Del Rosario, R., (2014) “A Future with Hybrid Electric Propulsion Systems: A NASA Perspective”, Turbine Engine Technology Symposium, 8-11 September 2014, Dayton, OH, United States [Online]. Available https://ntrs.nasa.gov/archive/nasa/casi.ntrs.nasa.gov/20150000748.pdf.

Donateo, T., Ficarella, A., Spedicato, L., (2018) "A method to analyze and optimize hybrid electric architectures applied to unmanned aerial vehicles", Aircraft Engineering and Aerospace Technology, Vol. 90 Issue: 5, pp.828-842, https://doi.org/10.1108/AEAT-11-2016-0202T.

Donateo, T., Ficarella, A., Spedicato, L., (2016) “Development and validation of a software tool for complex aircraft powertrains”, Advances in Engineering Software, 96, pp. 1-13. ISSN: 09659978 DOI: 10.1016/j.advengsoft.2016.01.001.

Donateo, T., De Pascalis, C.L., Ficarella, (2019) “A. Synergy Effects in Electric and Hybrid Electric Aircraft”, Aerospace 2019, 6, 32.

Donateo, T., Spedicato, L. (2017) “Fuel economy of hybrid electric flight”, Appl. Energy, 206, 723–738.

Emmerich, M., Beume, N., Naujoks, B., (2005) “An EMO Algorithm Using the Hypervolume Measure as Selection Criterion”, in Proceedings of the Third International Conference of Evolutionary Multi-Criterion Optimization EMO 2005, Guanajuato, Mexico, 9–11 March 2005.

Fletcher, S., Flynn, M.C., Jones, C.E. and Norman, P.J., (2016) “Hybrid electric aircraft: State of the art and key electrical system challenges”, IEEE Transportation Electrification eNewsletter, September 2016.

Frosina, E.; Senatore, A.; Palumbo, L.; Di Lorenzo, G.; Pascarella, C. Development of a Lumped Parameter Model for an Aeronautic Hybrid Electric Propulsion System. Aerospace 2018, 5, 105.

Guzzella, L., Sciarretta, A., (2007) “Vehicle Propulsion Systems: Introduction to Modeling and Optimization” Springer, Berlin, Germany.

Harmon F.H., Frank A. A., Joshi S. S., “Application of a CMAC Neural Network to the Control of a Parallel Hybrid-Electric Propulsion System for a Small Unmanned Aerial Vehicle”, Proceedings of International Joint Conference on Neural Networks, Montreal, Canada. July 31 - August 4, 2005.

ICAO, Document 9963 (2010), “Report of the Independent Experts on the Medium and Long Term Goals for Aviation Fuel Burn Reduction from Technology”, Montreal.

Lu Y., an J., Fan B., Otchere P., Chen W., Cheng B., (2019), “Research on the application of aviation kerosene in a direct injection rotary engine-Part 1: Fundamental spray characteristics and optimized injection strategies”, Energy Conversion and Management Volume 195, 1 September 2019, Pages 519-532

McCormick B. W., (1995) “Aerodynamics, Aeronautics and Flight Mechanics”, John Wiley, 1995.

Oron H., (2006) “UAV Engines in the next decade – Turbine Engines, Piston Engines and the newly Combat Proven Rotary Engine”, A lecture at the 6th Symposium on Jet Engines and Gas Turbines, Haifa, 16 November 2006.

Pornet C., Isikveren A.T., (2015) “Conceptual design of hybrid-electric transport aircraft”, Progress in Aerospace Sciences, 79, pp 114-135, DOI: http://dx.doi.org/10.1016/j.paerosci.2015.09.002.

Sarveswaran, V., Murthy (IN), Y., Ganesan, V., (2003) "Altitude Performance Comparison of A Wankel Engine With Carburetor and Fuel Injection," SAE Technical Paper 2003-28-0017, 2003, doi:10.4271/2003-28-0017.

Silvas E., Hofman R., Murgovsk N., Etman P., Steinbuch M. (2016), “Review of Optimization Strategies for System-Level Design in Hybrid Electric Vehicles”, IEEE Transactions on Vehicular Technology, pp 1-15.

Serrao L. (2009) “A comparative analysis of energy management strategies for hybrid electric vehicles”, Ph.D. Thesis, The Ohio State University.

Traub L. W. (2011), “Range and Endurance Estimates for Battery-Powered Aircraft”, Journal of Aircraft, Vol. 48, No. 2.

https://aviationweek.com/bca/jet-and-avgas-fuel-prices-august-2015 (accessed 06 June 2019)

https://ecometrica.com/assets/Electricity-specific-emission-factors-for-grid-electricity.pdf (accessed 06 June 2019)

https://www.epa.gov/sites/production/files/2015-07/documents/emission-factors_2014.pdf (accessed 06 June 2019)

https://www.globalpetrolprices.com/electricity_prices/ (accessed 06 June 2019)

http://kokam.com/cell/ (accessed 15 May 2019)

https://uavenginesltd.co.uk/products/ar682-75-bhp/ (accessed 05 June 2019)